Construction and Validation of a Prognostic Model Based on Mitochondrial Genes in Prostate Cancer

Authors
Dan Wang[1], Hui Pan[2], Shaoping Cheng[2], Zhigang Huang[2], Zhenlei Shi[2], Hao Deng[2], Junwu Yang[2], Chenghua Jin[2], Jin Dai[2] ⓘ

Affiliations
1   Radiology, The First Affiliated Hospital of Yangtze University, Jingzhou, China
2   Urology, The First Affiliated Hospital of Yangtze University, Jingzhou, China

Correspondence
Dr. Jin Dai
Urology, The First Affiliated Hospital of Yangtze University
No.55 North Jianghan Road
434000 Jingzhou
China
DDDaiJJJin@163.com

ABSTRACT

This study attempted to build a prostate cancer (PC) prognostic risk model with mitochondrial feature genes. PC-related MTGs were screened for Cox regression analyses, followed by establishing a prognostic model. Model validity was analyzed via survival analysis and receiver operating characteristic (ROC) curves, and model accuracy was validated in the GEO dataset. Combining risk score with clinical factors, the independence of the risk score was verified by using Cox analysis, followed by generating a nomogram. The Gleason score, microsatellite instability (MSI), immune microenvironment, and tumor mutation burden were analyzed in two risk groups. Finally, the prognostic feature genes were verified through a q-PCR test. Ten PC-associated MTGs were screened, and a prognostic model was built. Survival analysis and ROC curves illustrated that the model was a good predictor for the risk of PC. Cox regression analysis revealed that risk score acted as an independent prognostic factor. The Gleason score and MSI in the high-risk group were substantially higher than in the low-risk group. Levels of ESTIMATE Score, Immune Score, Stromal Score, immune cells, immune function, immune checkpoint, and immunopheno score of partial immune checkpoints in the high-risk group were significantly lower than in the low-risk group. Genes with the highest mutation frequencies in the two groups were SPOP, TTN, and TP53. The q-PCR results of the feature genes were consistent with the gene expression results in the database. The 10-gene model based on MTGs could accurately predict the prognosis of PC patients and their responses to immunotherapy.

Introduction

Prostate cancer (PC) is caused by malignant proliferation of prostate epithelial cells and its incidence is the second highest among male malignancies worldwide, with nearly 1.4 million new cases and 375 000 deaths in 2020 [1, 2]. Increased age, family history of malignancy, genetic mutations, and dietary factors are possible risk factors and causes of PC [1, 2]. Surgery and radiotherapy are the standard of care for PC [3]. Most PC patients who have escaped from cancer spreading have a 5-year survival rate close to 100 %

after treatment, but the 5-year survival rate for PC patients diagnosed with spread cancer is 31 % (https://www.cancer.net/cancer-types/prostate-cancer/statistics). For patients with metastatic PC, androgen deprivation therapy (ADT) is commonly used, but drug resistance limits the use of this treatment [4]. In recent years, hormone therapy, chemotherapy, targeted therapy, immunotherapy, and other treatment methods have been developed and applied to patients with advanced or metastatic PC, but the efficacy is still not satisfactory [5]. Therefore, finding new markers to accu-

rately predict the prognosis of patients will benefit the precision treatment of patients with PC.

Mitochondria are highly dynamic organelles, and mitochondrial fission and fusion are key players in energy production, cell cycle, and immune and apoptotic pathways [6]. In highly aggressive tumor cells, the mitochondrial energy pathway is reprogrammed to allow cancer cells to utilize energy better for macromolecular synthesis for rapid cancer cell division and migration [7]. Chang et al. [8] reported that transplantation of mitochondrial DNA from healthy individuals into breast cancer cell lines suppresses cancer cell proliferation, induces caspase-dependent and apoptosis-inducing factor (AIF) protein-mediated apoptosis, and can also increase chemotherapy sensitivity. Somatic mutations in the mitochondrial genome are common in PC patients [9]. Hopkins et al. [10] disclosed that mitochondrial mutations and nuclear mutations are positively correlated with PC aggressiveness, and varying mitochondrial somatic mutation genes are involved in various survival outcomes of PC. Moreover, mitochondria influence immune surveillance through both intrinsic and exogenous mechanisms of cancer cells. Mitochondrial metabolism plays a role in multiple anticancer immune functions, including (but not limited to) inflammasome activation, the formation of protective immune memory, and the differentiation and tumor-killing activity of specific macrophage subpopulations [11]. Jin et al. [12] described the use of small molecule inhibitors in targeting mitochondria to overcome cancer chemotherapy resistance. In conclusion, mitochondria are critical in PC tumorigenesis and progression and are potentially likely prognostic factors.

In this work, clinical data of PC patients in The Cancer Genome Atlas (TCGA) were processed, and mitochondrial genes (MTGs) that influenced the survival of PC patients were identified by Cox regression analysis. A prognostic risk model for PC based on MTGs was eventually developed. The predictive performance of this model was validated in the Gene Expression Omnibus (GEO) dataset, and a nomogram was built for predicting PC patients' prognoses in conjunction with clinical information. This study developed a new prognostic model for risk assessment of PC to generate insight into disease progression and treatment of PC patients.

Materials and Methods

Data downloading

We downloaded all data related to PC (normal: n = 52; tumor: n = 501) from TCGA (https://portal.gdc.cancer.gov/) as the training set. GSE116918 (platform: GPL25318) and GSE70769 from GEO (https://www.ncbi.nlm.nih.gov/geo/) were set as validation sets, containing gene expression profiles and clinical information from 248 primary PC patients. MitoCarta 3.0 database contained 1136 human and 1140 mouse protein-coding genes that were localized to the mitochondria and provided annotation information on the submitochondrial localization of genes. A set of 1136 human MTGs were downloaded from the MitoCart 3.0 database (http://www.broadinstitute.org/mitocarta).

Screening for MTGs associated with PC

Differential analysis of gene expression between healthy and PC samples in TCGA (FDR < 0.05, |logFC| > 0.585) was completed by R package "edgeR" [13]. Intersection of differentially expressed genes (DEGs) of PC and MTGs was taken to screen out differentially expressed MTGs in PC for model establishment.

Screening for prognostic markers and establishment of a model

Univariate Cox regression analysis of PC-related MTGs was completed using the R package "survival" (https://github.com/therneau/survival) to screen out key MTGs (p < 0.05). LASSO regression and multivariate Cox regression analyses were completed by R package "glmnet" [14] and "survival", and the final retained genes were utilized to establish a PC prognostic model.

Assessment of model predictive performance and validation on the GEO dataset

The median value of risk score was set as the threshold value and used to assign samples into high- and low-risk groups. Maps of risk score distributions and survival status and heat maps of expression levels were generated for samples in two groups. Kaplan–Meier (KM) survival curves were generated by the R package "survival". The 3-year and 5-year ROC curves for training set samples were generated using R packages "timeROC" [15] and "survival". The 3-year and 5-year AUC values were calculated to assess model accuracy.

The GSE116918 dataset was normalized using the R package "limma" [16]. To determine the model validity, maps of risk score distributions and survival status, heat maps of expression levels, KM survival curves, 3-year and 5-year ROC curves, and AUC values were plotted for two groups in the validation set.

Independent prognosis analysis

The R packages "survival" and "forest plot" (https://cran.r-project.org/web/packages/forestplot/vignettes/forestplot.html) were employed to conduct univariate and multivariate Cox regression analyses of major prognostic factors such as age, T, N, Gleason_score, and risk score in PC patients in the training set. R package "rms" [17] and "survival" were utilized to draw a prognostic nomogram. Calibration curves were generated using the R package "rms" to evaluate the agreement between the overall survival (OS) predicted by the nomogram and the actual OS.

Analysis of risk score with Gleason score and microsatellite instability (MSI)

Samples were grouped according to clinical factors (T, N, Gleason score) from TCGA. The Wilcox test was performed on two risk groups to analyze whether a difference exists in risk score among these clinical factors. R package "vioplot" (https://github.com/TomKellyGenetics/vioplot) was utilized to draw violin plots. The Wilcox test was to analyze whether there was a difference in MSI Score MantiS and MSI Sensor Score between the two groups and generated violin plots.

Gene ontology (GO) and Kyoto encyclopedia of genes and genomes (KEGG) enrichment analyses

A threshold value (FDR < 0.01, |logFC| > 1) was set, and genes differing between the two groups were screened by the R package "edgeR". Enrichment analysis was conducted by R package "clusterProfiler" [18] to investigate changes in biological functions and related pathways between two groups.

Single sample gene set enrichment analysis (ssGSEA)

The ESTIMATE Score, Immune Score, Stromal Score, and Tumor Purity of each sample were computed by R package "estimate" [19] for the Wilcox test and violin plot. The R package "GSVA" [20] was utilized to compare levels of immune-related cells, immune-related functions, and immune checkpoint genes in two risk groups. The Wilcox test was used to compare differences between the two groups and the results were presented using violin and box plots. The immunophenoscore (IPS) of PC was accessed from the Cancer Immunome Atlas (TCIA; https://tcia.at) to analyze differences in IPS between two risk groups.

Analysis of tumor mutation burden (TMB)

Differences in mutation data between two risk groups were analyzed by R package "maftools" (https://github.com/PoisonAlien/maftools), followed by analyses of mutated genes in high- and low-risk groups separately.

Cell culture

Human normal prostatic epithelial cells RWPE-1 (CTCC-003-0013) and human PC cells C4-2B (CTCC-001-0417), as well DU145 (CTCC-001-0013), were purchased from MEISEN CELL. All the above cell lines were cultured in RPMI-1640 medium supplemented with 10% fetal bovine serum (FBS) at 37 °C in a 5% CO_2 incubator.

qRT-PCR

Total RNA was extracted from cells using Trizol reagent (Invitrogen, USA) and reversely transcribed into cDNA. cDNA was used as a template for PCR amplification using the One Step SYBR PrimeScript RT-PCR Kit (Takara, Japan). PCR was performed using a fluorescent quantitative PCR instrument. Gene expression levels were quantitatively calculated by the $2^{-\Delta\Delta Ct}$ method. GAPDH was the internal reference. Primer sequences are shown in ▶ Table 1.

Statistical analysis

Each experiment for qRT-PCR was repeated at least three times. Data were analyzed using GraphPad Prism 8.0 software. A comparison between the two groups was conducted by Student's *t*-test. A p-value of < 0.05 was considered a significant difference.

Results

Screening for PC-related MTGs

A total of 5608 DEGs were identified in 52 normal tissues and 501 PC tumor tissues, and 1136 MTGs were downloaded. After taking the intersection of DEGs and MTGs, 231 differentially expressed MTGs in PC were screened (**Supplementary Fig. 1S**), which were target genes in this study.

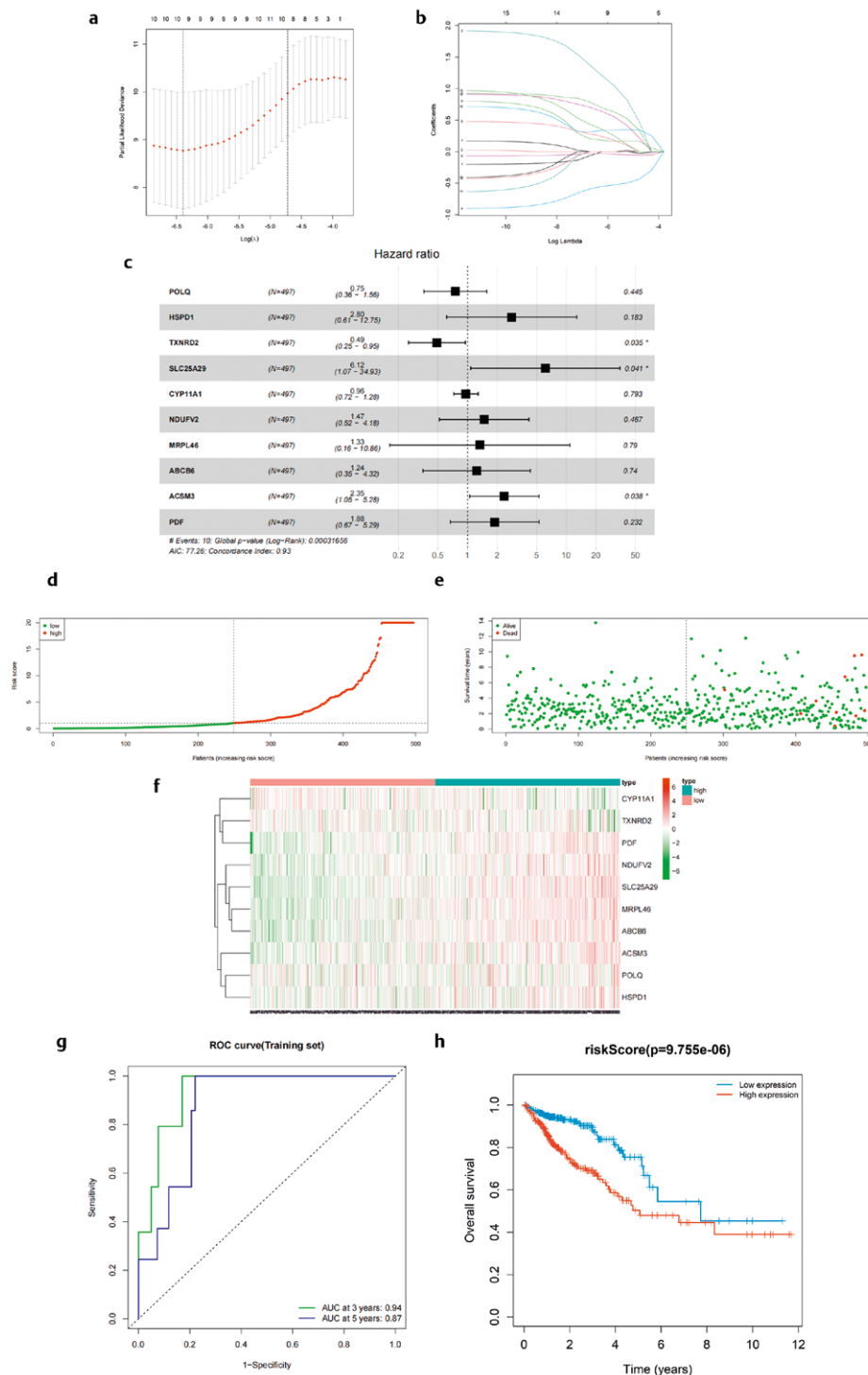## Establishment and validation of the model

The correlation between differentially expressed MTGs in PC and OS in PC patients was analyzed by univariate Cox regression analysis. Fifteen PC-related MTGs were screened according to the threshold (p < 0.05) (**Table 1S**), and they were subsequently included in LASSO regression analysis. Ten genes were finally screened (POLQ, HSPD1, TXNRD2, SLC25A29, CYP11A1, NDUFV2, MRPL46, ABCB6, ACSM3, PDF) (▶ **Fig. 1a, b**). Multivariate Cox regression analysis was performed, and no genes were excluded (▶ **Fig. 1c**). Finally, by multiplying the expression of each gene by coefficients from multivariate Cox regression, the prognostic model was established:

$$Riskscore = -0.2848 * POLQ + 1.0293 * HSPD1 - 0.7123 * TXNRD2 + 1.8119$$
$$* SLC25A29 - 0.0382 * CYP11A1 + 0.3873 * NDUFV2 + 0.2854 * MRPL46$$
$$+ 0.2116 * ABCB6 + 0.8557 * ACSM3 + 0.6314 * PDF$$

Samples were assigned into high- and low-risk groups based on the median risk score. Risk score distribution (▶ **Fig. 1d**), survival

▶ **Table 1** Primer sequences for qRT-PCR.

Primer sequences (5′–3′)		
POLQ	GCCAGGGTTCTCTATGCTTC	TCTTCAACTGCTTCCTCTTCC
HSPD1	AGTCCATTGTACCTGCTCTTG	TGACTGCCACAACCTGAAG
TXNRD2	AGATCTGATGGACTACGACAATG	CAGTGGTTTATAATGGGCGTG
SLC25A29	CTGGACTTCTTGGCTGGATG	TGATGGACTTGAAGCAGTGC
CYP11A1	AAGTCCACCTTCACCATGTC	TGAGGAATCGTTCTGGGTTG
NDUFV2	GGCAAAATCCCAAAACCAGG	TGCTTGTACACCAAATCCAGG
MRPL46	TTGGAAGATATGTGGGAGCAG	CTGACTAACAGGACAAGGTTCC
ABCB6	CTCATTGTGTTCCTGTGCATG	TTCACCGTCTCGAAGTTTAGC
ACSM3	ATGGAGAAACAAGACGGGC	ACATCGAAAGCAGGAGAAGG
PDF	CGTGTTCGTGAACCCCAG	CCACCTGTTCTCCATTGGG
GAPDH	CAATGACCCCTTCATTGACC	GACAAGCTTCCCGTTCTCAG

▶ Fig. 1 Establishment and validation of the PC prognostic model. **a**: Distribution of cross-validation results for adjusting the penalty parameter λ in the LASSO model; **b**: Distribution of the coefficient spectrum of the feature genes with the penalty parameter λ; **c**: Forest plot of multivariate Cox regression analysis of 10 PC-related MTGs; **d**: Risk score distribution map. Green: low risk; red: high risk; **e**: Scatter plots of survival time and survival status for two risk groups. Green: alive; red: dead; **f**: Heat map of expression of 10 feature genes in two risk groups. The color from green to red represents the progressive increase in gene expression; **g**: ROC curves; **h**: Survival curves. Blue: low-risk group; red: high-risk group.

status (▶ **Fig. 1e**), and expression level heat map (▶ **Fig. 1f**) were plotted. The results suggested that risk score could clearly distinguish high- and low-risk groups. The 3-year and 5-year ROC curves were generated, and AUC values were calculated. The 3-year and 5-year AUC values were 0.94 and 0.87, respectively (▶ **Fig. 1g**), indicating favorable predictive performance of the prognostic model. Survival analysis revealed a higher survival rate in the low-risk group than in the other group (▶ **Fig. 1h**).

To verify whether the model also has good predictive performance in other datasets, the GEO dataset GSE116918 and GSE70769 were utilized as the validation set for analysis. The risk score distribution map (**Supplementary Fig. 2AS**), survival status map (**Supplementary Fig. 2BS**), and expression level heat map (**Supplementary Fig. 2CS**) were plotted in the validation set based on samples from two risk groups. The 3-year and 5-year ROC curves

were generated, and AUC values were calculated (**Supplementary Fig. 2DS, 2FS**). The 3-year and 5-year AUC values were 0.7 and 0.72, respectively. Survival analysis revealed that OS was higher in the low-risk group than in the other group in the validation set (**Supplementary Fig. 2ES, 2GS**). Taken together, the 10-gene PC prognostic model had favorable predictive performance in training and validation sets.

Independent prognostic analysis

Combining clinical information (age, T, N, Gleason_score) of PC samples, univariate and multivariate Cox regression analyses were conducted on risk score and clinical information. Univariate Cox regression analysis illustrated that T, N, Gleason_score, and risk score may be independent prognostic factors for PC (▶ **Fig. 2a**). In multivariate Cox regression analysis, only risk score was a prognostic
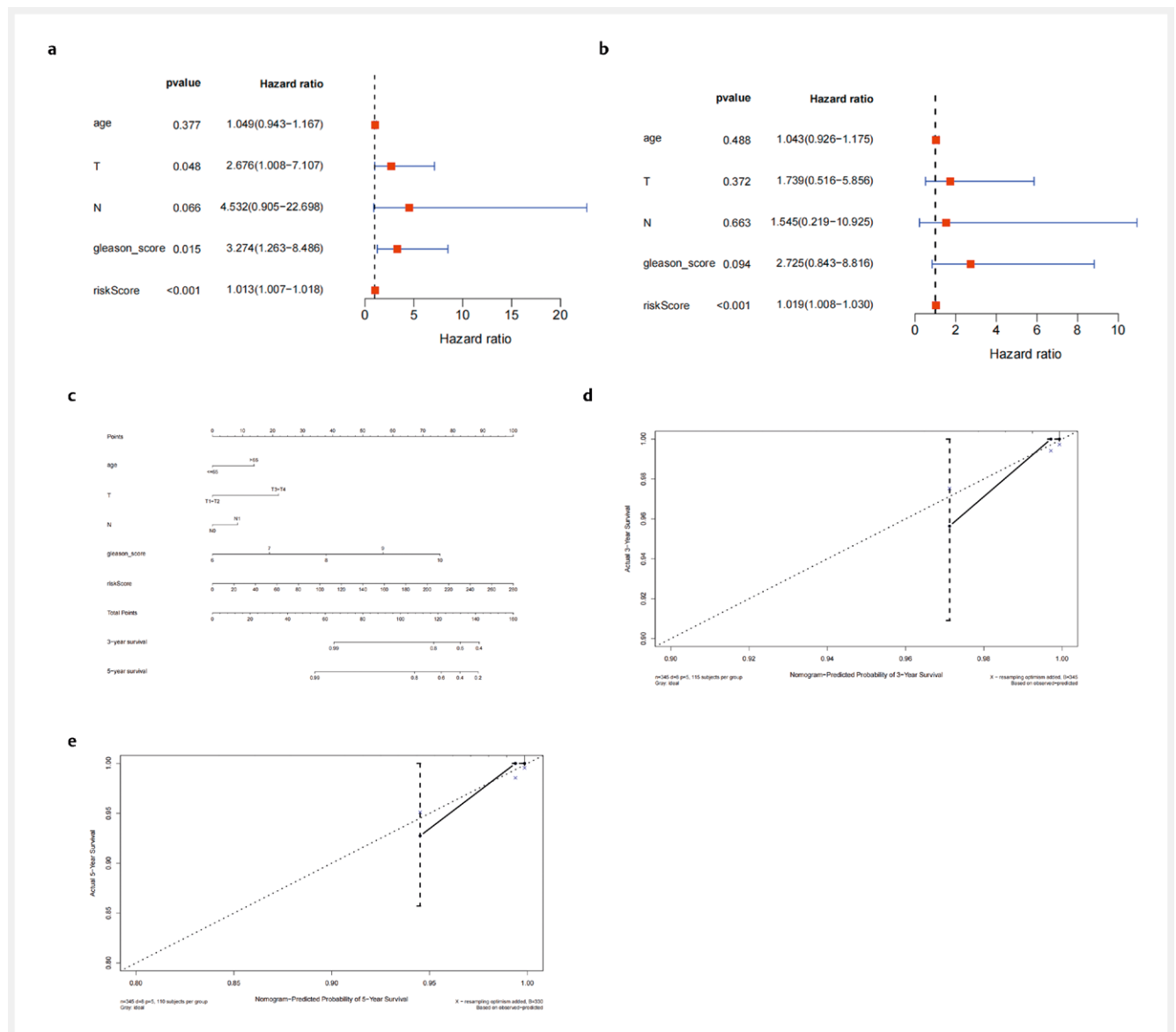
▶ **Fig. 2** Risk score independent prognostic analysis. **a**: Forest plot of univariate Cox regression analysis; **b**: Forest plot of multivariate Cox regression analysis; **c**: Nomogram of prognostic model risk score combined with clinical information; **d**: The predicted 3-year OS calibration curve; **e**: The predicted 5-year OS calibration curve.

factor for PC (▶ **Fig. 2b**). These findings indicated that risk score was an independent prognostic factor for PC.

To help clinicians apply the model preferably, a nomogram was generated based on risk score and clinical information (▶ **Fig. 2c**). The 3-year and 5-year calibration curves presented that the nomogram-predicted OS was in close proximity to the actual OS (▶ **Fig. 2d–e**), indicating the favorable predictive performance of the nomogram.
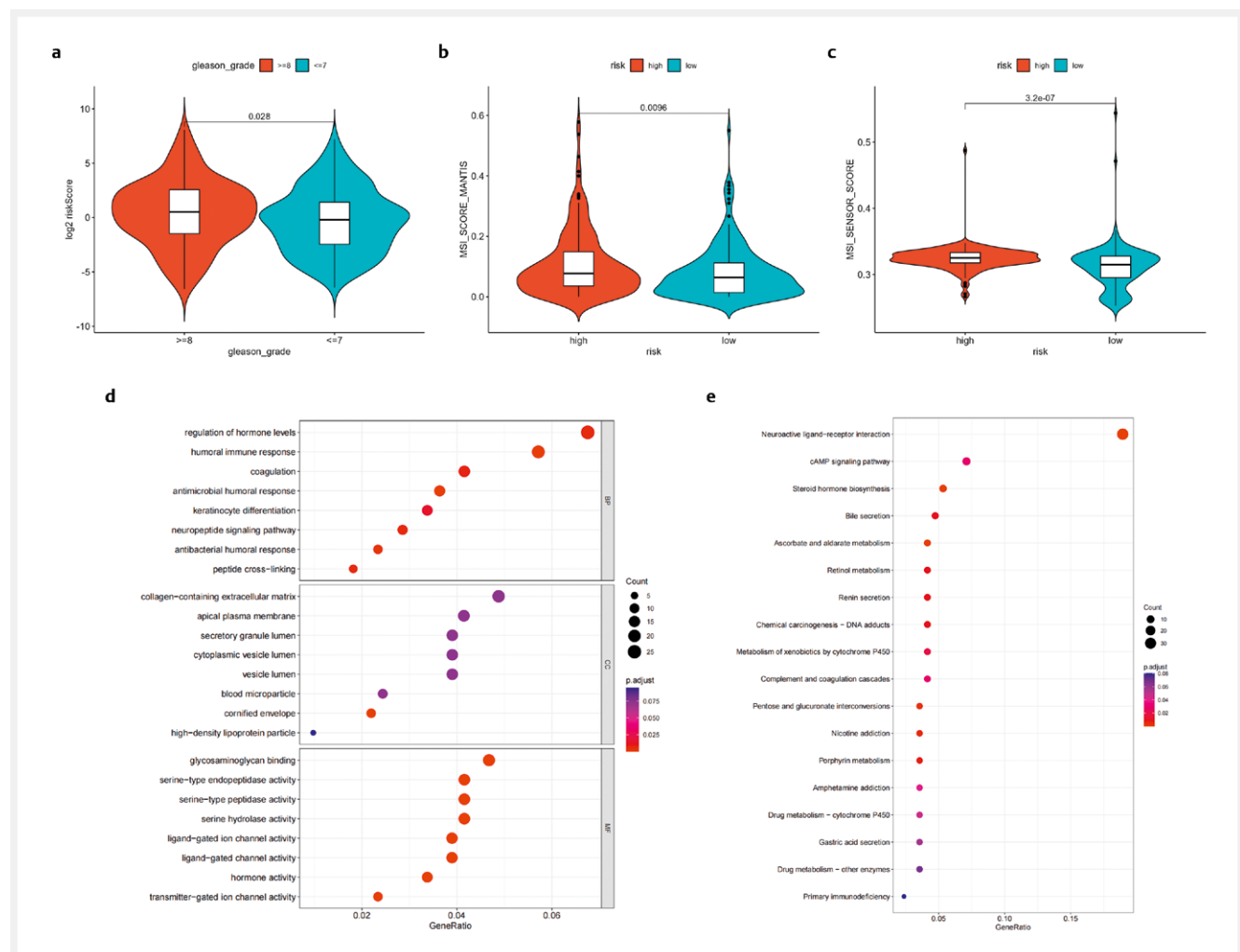
Gleason score and MSI analysis

The Wilcox test was conducted on risk score using Gleason_score and MSI. The Gleason score indicated the malignant degree of PC, with a score range of 2–10, and a higher score presented a poorer differentiation and higher malignancy of PC, meaning a worse prognosis for the patient. The risk score distinguished patients with varying Gleason scores, and it was higher in the advanced stage of cancer than in the early and middle stages (▶ **Fig. 3a**). The MSI Score Mantis and MSI Sensor Score were also substantially different in the

two risk groups, with the high-risk group having higher scores and unstable microsatellite sequences (▶ **Fig. 3b, c**). These data suggested that risk score had clinical significance.

Subsequently, differential analysis of the high- and low-risk groups yielded 436 DEGs, which were subjected to GO and KEGG enrichment analyses. GO results presented the enrichment of these genes in biological functions like regulation of hormone levels, humoral immune response, coagulation, glycosaminoglycan binding, and serine-type endopeptidase activity (▶ **Fig. 3d**). KEGG results presented the enrichment of these genes on pathways like Neuroactive ligand-receptor interaction, cAMP signaling pathway, and Steroid hormone biosynthesis (▶ **Fig. 3e**).

ssGSEA

The ratio of immune cells and stromal cells in tumors had a notable influence on prognosis, and ESTIMATE Score, Immune Score, Stromal Score, and Tumor Purity were calculated for each sample. The results illustrated that compared to the high-risk group, the

▶ **Fig. 3** Gleason score and MSI analysis. **a**: Differential analysis of Gleason score in high- and low-risk groups. Gleason score ≥ 8 indicates advanced PC and Gleason score ≤ 7 indicates early to middle-stage PC; **b**: Differential analysis of MSI Score Mantis. MSI represents the satellite instability, and a higher MSI Score means a higher degree of instability of the satellite; **c**: Differential analysis of MSI Sensor Score in high- and low-risk groups. MSI Sensor is the software that detects satellite instability, and a higher score means a higher degree of instability of the satellite; **d**: Results of GO enrichment analysis; **e**: Results of KEGG enrichment analysis.
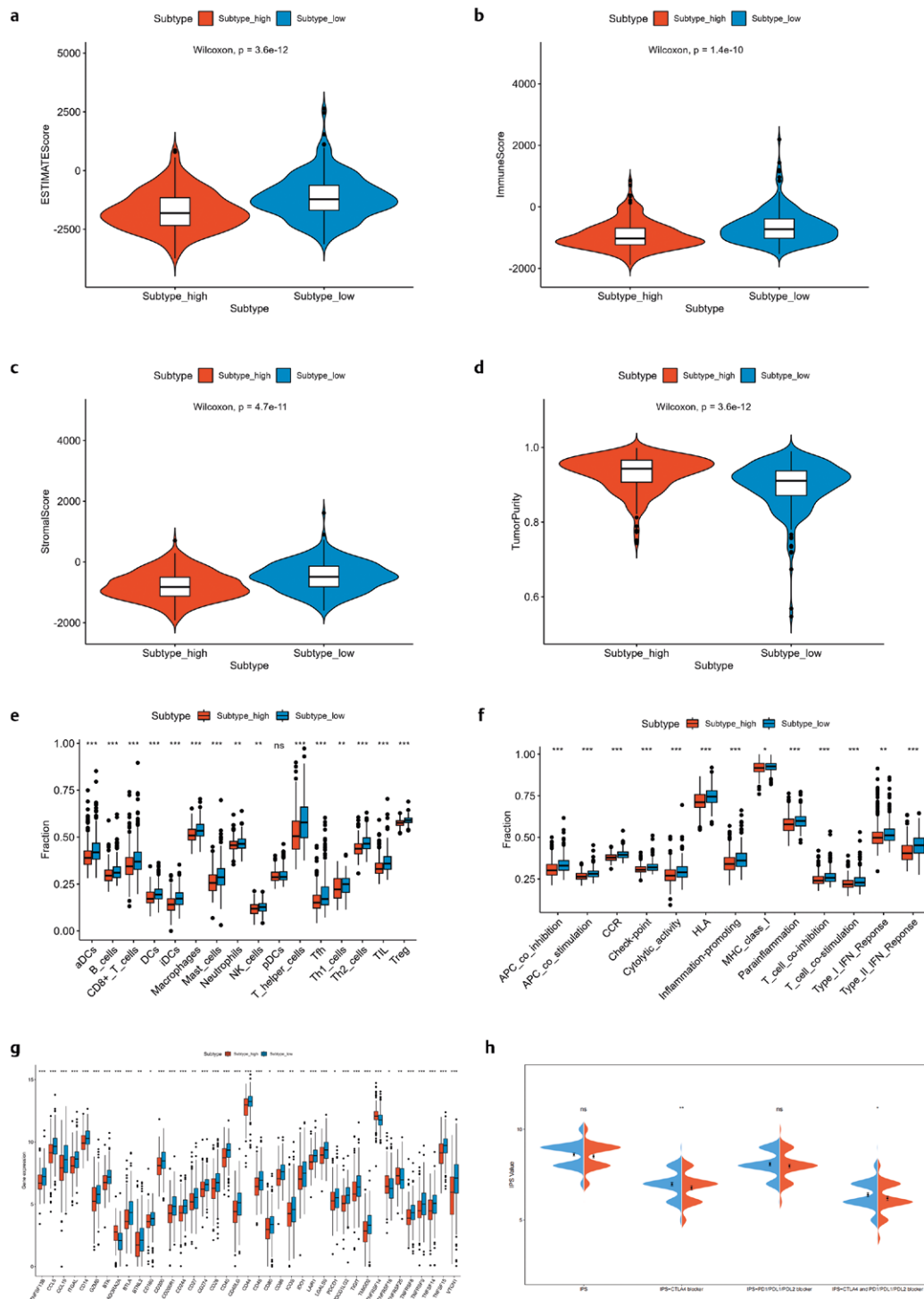
▶ **Fig. 4** Immune microenvironment analysis of high- and low-risk groups. **a**: ESTIMATE Score differential analysis; **b**: Immune Score differential analysis; **c**: Stromal Score differential analysis; **d**: Tumor Pext-linkty differential analysis; **e**: Differential analysis of immune cells in high- and low-risk groups; **f**: Differential analysis of immune function in high- and low-risk groups; **g**: Differential analysis of immune checkpoints in high- and low-risk groups; **h**: Differential analysis of IPS in high- and low-risk groups; *p<0.05; * *p<0.01; * * *p<0.001.
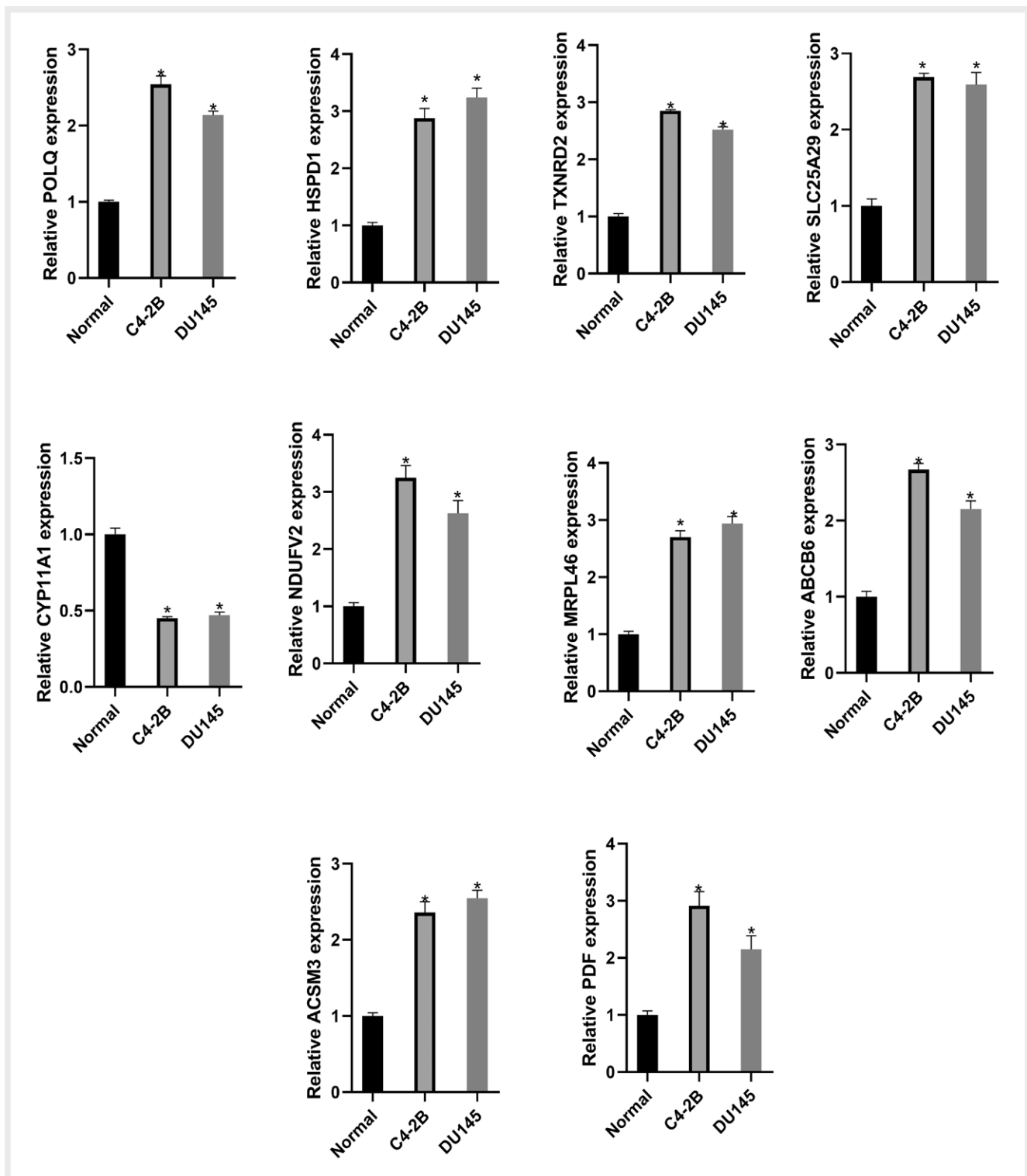
▶ **Fig. 5** q-PCR results of prognostic genes; * p < 0.05.

ESTIMATE Score, Immune Score, and Stromal Score were substantially upregulated in the low-risk group (p < 0.05) (▶ **Fig. 4a–c**). Tumor Purity was significantly downregulated in the low-risk group but not in high-risk group (p < 0.05) (▶ **Fig. 4d**).

To assess the immune infiltration in samples, R package "GSVA" was utilized to assess the immune infiltration level in each PC sam-

ple. Immune infiltration levels of aDCs, B_cells, CD8 + _T_cells, macrophages, and Treg in the high-risk group were notably lower than in the other group (p < 0.05), except for the immune infiltration level of pDCs, which was not significantly different (▶ **Fig. 4e**). Among the immune functions, HLA, MHC_class_I, and para-inflammation in the high-risk group were substantially lower than in the

other group (p < 0.05) (▶ **Fig. 4f**). Assessment of differences in immune checkpoints revealed that the expression levels of all immune checkpoints, including PDCD1, CTLA4, and LAG3, were remarkably upregulated in the low-risk group but not in the high-risk group (▶ **Fig. 4g**). Higher IPS indicated a better response to immunotherapy. Differential analysis plots of IPS in the two groups showed that the IPS-CTLA4 blocker, IPS-CTLA4, and PD1/PDL1/PDL2 blocker in the high-risk group were substantially lower than in the other group (▶ **Fig. 4h**), thus indicating that PC patients in the low-risk group were more potential to benefit from immunotherapy.

TMB analysis

Analysis of TMB in two groups unveiled that the number of TMB in the high-risk group was conspicuously higher than in the other group (p < 0.05) (**Supplementary Fig. 3AS**). Subsequent mapping of the TMB waterfall plots in high- and low-risk groups respectively presented that SPOP, TTN, and TP53 were the top 3 mutated genes in PC patients in both groups (**Supplementary Fig. 3BS**, **CS**), but there were more FOXA1 mutations in the low-risk group and more LRP1B mutations in the high-risk group.

Expression level validation of prognostic feature genes

We further validated the expression levels of the model feature genes in PC cells using qRT-PCR. The validation results were consistent with the previous analysis of gene expression in the database. Except for CYP11A1, all other prognostic feature genes were up-regulated in PC cells (▶ **Fig. 5**).

Discussion

PC is the second leading cause of cancer-associated deaths in men in developed countries, and patients with late diagnoses or metastases are refractory to conventional treatments [21]. Prognostic markers facilitate personalized treatment of PC patients to maximize therapeutic effects [22]. Mitochondria are organelles essential for tumor growth and provide a range of key substances for tumor cell metabolism [23]. Li et al. [24] revealed that p53/PGC-1α-mediated mitochondrial dysfunction drives PC cell apoptosis. Pecinová et al. [25] reported that PC cells are correlated with high activity of mGPDH, and mGPDH overexpression enhances PC cell migratory potential. In this work, a 10-gene prognostic model was built for PC patients based on MTGs.

DEGs of PC from TCGA were intersected with MTGs, and key genes were then identified by Cox regression analysis to establish a 10-gene PC risk prognostic model (POLQ, HSPD1, TXNRD2, SL-C25A29, CYP11A1, NDUFV2, MRPL46, ABCB6, ACSM3, PDF). Through q-PCR experiments, it was found that all other prognostic feature genes were up-regulated in PC cells, except CYP11A1, which was consistent with the results in the database. POLQ, a DNA polymerase involved in manipulating the cell cycle, catalyzes DNA double-stranded unwinding and participates in the DNA repair process of the organism [26]. POLQ is barely detectable in non-tumor tissues, but it is highly expressed in gastric, lung, and colon cancers, and its overexpression may contribute to tumor progression [27]. Jia et al. [28] revealed that POLQ is upregulated in patients with metastatic castration-resistant PC (mCRPC) and is implicated

in poor prognosis; in addition, POLQ targeting mCRPC patients enhances the anticancer effects of docetaxel chemotherapy. HSPD1 is a protective protein that protects intracellular proteins against misfolding or aggregation, inhibits cell death signaling cascade response, and preserves intracellular signaling pathways essential for cell survival [29]. The heat shock protein (HSP) family is pivotal in cell proliferation, differentiation, and tumorigenesis, and it is a biomarker for cancer diagnosis and a target for disease progression assessment or cancer treatment [30]. Song et al. [31] disclosed that HSP27, ALDH6A1, and Prohibitin act together to forecast the survival of patients with metastatic PC. CYP11A1 belongs to the steroid CYP gene family and encodes cytochrome P450scc (cholesterol side-chain cleavage enzyme). CYP11A1 is responsible for catalyzing the first and rate-limiting step in steroidogenesis and conversing cholesterol to pregnenolone [32]. Maksymchuk et al. [33] found that CYP11A1 is not expressed in normal prostate tissue and is strongly linked with the development of aggressive PC. Zhang et al. [34] reported that NDUFV2 is involved in androgen regulation, and it is an unfavorable prognostic marker for PC. Karatas et al. [35] disclosed that ABCB6 expression is substantially upregulated in PC tissue and recurrent PC compared to normal prostate tissue and holds prognostic value. MRPL46 is a protein-coding gene whose associated pathways contain mitochondrial translation and protein metabolism. Antony et al. [36] presented that MRLP46, BCOR, and CREB3 are implicated in prognoses of ovarian cancer patients. Zhang et al. [37] reported that aberrant upregulation of SL-C25A29 contributes to the transport of arginine to mitochondria and improves mitochondria-derived NO levels, thereby manipulating metabolic status and driving cancer progression. Zhao et al. [38] illustrated that ACSM3 plays a role in several cancers and is substantially downregulated in malignant melanoma; additionally, targeting ACSM3 hampered melanoma progression. These investigations suggested that the screened genes manipulate tumorigenesis and progression of PC and other cancers, counting for PC patient's prognostic prediction.

In the immune microenvironment, immune infiltration in the PC high-risk group was substantially lower than in the other group, and a large number of immune cells such as Tregs and macrophages were markedly downregulated in the high-risk group. Tregs dysfunction is a major cause of autoimmune and inflammatory diseases of the organism [39]. High infiltration of Tregs in the tumor microenvironment is implicated in dismal prognoses of patients with varying cancers [40]. Unlike these studies, Tregs were highly expressed and indicated a good prognosis in low-risk patients in the present study. Ohue et al. [40] reported that Tregs have different classifications, in which antigen-specific Tregs cells play superior immunosuppressive roles relevant to antigen-nonspecific Tregs cells, which may be a reason why the results of this study differ from other studies. In this work, only the total Tregs of two risk groups were compared. Liu et al. [41] presented that M2 macrophages drive PC progression and contribute to the establishment of an immunosuppressive state in tumors. However as revealed in this work, macrophages were notably lower in patients in the high-risk group, which may be related to macrophage typing. In addition, expression levels of all immune checkpoints in the PC high-risk group were substantially lower than in the other group. PDCD1 overexpression is a strategy for tumor cells to evade immune surveillance and high-

er expression of PDCD1 is seen in aggressive PC and is implicated in dismal prognosis [42]. Patients with high PD-L1 expression in tumors appear to be more likely to benefit from anti-PDCD1 therapy [43]. CTLA-4 diminishes anti-tumor immune responses by producing inhibitory signals to reduce T cell activation [44]. Waitz et al. [45] manifested that combined thermal ablation of CTLA-4 blockade for PC enhances antitumor immunity and tumor metastasis rejection. Hence, it is clear that patients with a low risk of PC who receive immunotherapy are prone to survive long-term.

Overall, the prognostic nomogram constructed based on MTGs had a favorable performance for predicting PC patients' survival. Immune microenvironment was analyzed to assess the immunotherapeutic effects on PC patients at different risks. But deficiencies exist. First, this work was based on bioinformatics analysis in public databases and the results were not evaluated in conjunction with clinical data. Thus, validation of the model through prospective studies is warranted. Second, the specific mechanism of the mitochondrial characteristic genes screened in this study in the prognosis of PC patients still needs to be further explored by experiments.

Conflict of Interest

The authors declare that they have no conflict of interest.

References

[1] Sung H, Ferlay J, Siegel RL et al. Global cancer statistics 2020: GLOBOCAN estimates of incidence and mortality worldwide for 36 cancers in 185 countries. CA Cancer J Clin 2021; 71: 209–249

[2] Matsushita M, Fujita K, Nonomura N. Influence of diet and nutrition on prostate cancer. Int J Mol Sci 2020; 21: 1447

[3] Testa U, Castelli G, Pelosi E. Cellular and molecular mechanisms underlying prostate cancer development: therapeutic implications. Medicines (Basel) 2019; 6: 82

[4] Jeong SH, Kwak C. Immunotherapy for prostate cancer: requirements for a successful regime transfer. Investig Clin Urol 2022; 63: 3–13

[5] Thomas TS, Pachynski RK. Treatment of advanced prostate cancer. Mo Med 2018; 115: 156–161

[6] Tilokani L, Nagashima S, Paupe V et al. Mitochondrial dynamics: overview of molecular mechanisms. Essays Biochem 2018; 62: 341–360

[7] Jia D, Park JH, Jung KH et al. Elucidating the metabolic plasticity of cancer: mitochondrial reprogramming and hybrid metabolic states. Cells 2018; 7: 21

[8] Chang JC, Chang HS, Wu YC et al. Mitochondrial transplantation regulates antitumour activity, chemoresistance and mitochondrial dynamics in breast cancer. J Exp Clin Cancer Res 2019; 38: 30

[9] Kloss-Brandstätter A, Schäfer G, Erhart G et al. Somatic mutations throughout the entire mitochondrial genome are associated with elevated PSA levels in prostate cancer patients. Am J Hum Genet 2010; 87: 802–812

[10] Hopkins JF, Sabelnykova VY, Weischenfeldt J et al. Mitochondrial mutations drive prostate cancer aggression. Nat Commun 2017; 8: 656

[11] Buck MD, Sowell RT, Kaech SM et al. Metabolic instruction of immunity. Cell 2017; 169: 570–586

[12] Jin P, Jiang J, Zhou L et al. Mitochondrial adaptation in cancer drug resistance: prevalence, mechanisms, and management. J Hematol Oncol 2022; 15: 97

[13] Robinson MD, McCarthy DJ, Smyth GK. edgeR: a bioconductor package for differential expression analysis of digital gene expression data. Bioinformatics (Oxford, England) 2010; 26: 139–140

[14] Friedman J, Hastie T, Tibshirani R. Regularization paths for generalized linear models via coordinate descent. J Stat Softw 2010; 33: 1–22

[15] Blanche P, Dartigues JF, Jacqmin-Gadda H. Estimating and comparing time-dependent areas under receiver operating characteristic curves for censored event times with competing risks. Stat Med 2013; 32: 5381–5397

[16] Ritchie ME, Phipson B, Wu D et al. Limma powers differential expression analyses for RNA-sequencing and microarray studies. Nucleic Acids Res 2015; 43: e47

[17] Huang C, Liu Z, Xiao L et al. Clinical significance of serum CA125, CA19-9, CA72-4, and fibrinogen-to-lymphocyte ratio in gastric cancer with peritoneal dissemination. Front Oncol 2019; 9: 1159

[18] Yu G, Wang LG, Han Y et al. clusterProfiler: an R package for comparing biological themes among gene clusters. Omics 2012; 16: 284–287

[19] Yoshihara K, Shahmoradgoli M, Martínez E et al. Inferring tumour purity and stromal and immune cell admixture from expression data. Nat Commun 2013; 4: 2612

[20] Hänzelmann S, Castelo R, Guinney J. GSVA: gene set variation analysis for microarray and RNA-seq data. BMC Bioinformatics 2013; 14: 7

[21] Lorenc T, Klimczyk K, Michalczewska I et al. Exosomes in prostate cancer diagnosis, prognosis and therapy. Int J Mol Sci 2020; 21: 2118

[22] Kretschmer A, Tilki D. Biomarkers in prostate cancer - current clinical utility and future perspectives. Crit Rev Oncol Hematol 2017; 120: 180–193

[23] Vasan K, Werner M, Chandel NS. Mitochondrial metabolism as a target for cancer therapy. Cell Metab 2020; 32: 341–352

[24] Li J, Li Y, Chen L et al. p53/PGC-1α-mediated mitochondrial dysfunction promotes PC3 prostate cancer cell apoptosis. Mol Med Rep 2020; 22: 155–164

[25] Pecinová A, Alán L, Brázdová A et al. Role of mitochondrial glycerol-3-phosphate dehydrogenase in metabolic adaptations of prostate cancer. Cells 2020; 9: 1764

[26] Yoshimura M, Kohzaki M, Nakamura J et al. Vertebrate POLQ and POLbeta cooperate in base excision repair of oxidative DNA damage. Mol Cell 2006; 24: 115–125

[27] Kawamura K, Bahar R, Seimiya M et al. DNA polymerase theta is preferentially expressed in lymphoid tissues and upregulated in human cancers. Int J Cancer 2004; 109: 9–16

[28] Kuei CH, Lin HY, Lin MH et al. DNA polymerase theta repression enhances the docetaxel responsiveness in metastatic castration-resistant prostate cancer. Biochim Biophys Acta Mol Basis Dis 2020; 1866: 165954

[29] Dubrez L, Causse S, Borges Bonan N et al. Heat-shock proteins: chaperoning DNA repair. Oncogene 2020; 39: 516–529

[30] Wu J, Liu T, Rios Z et al. Heat shock proteins and cancer. Trends Pharmacol Sci 2017; 38: 226–256

[31] Cho SY, Kang S, Kim DS et al. HSP27, ALDH6A1 and prohibitin act as a trio-biomarker to predict survival in late metastatic prostate cancer. Anticancer Res 2018; 38: 6551–6560

[32] Lin YC, Papadopoulos V. Neurosteroidogenic enzymes: CYP11A1 in the central nervous system. Front Neuroendocrinol 2021; 62: 100925

[33] Maksymchuk OV, Kashuba VI. Altered expression of cytochrome P450 enzymes involved in metabolism of androgens and vitamin D in the prostate as a risk factor for prostate cancer. Pharmacol Rep 2020; 72: 1161–1172

Zhang H, Shao Y, Chen W et al. Identifying mitochondrial-related genes NDUFA10 and NDUFV2 as prognostic markers for prostate cancer through biclustering. Biomed Res Int 2021; 5512624. doi:10.1155/2021/5512624

[34] Karatas OF, Guzel E, Duz MB et al. The role of ATP-binding cassette transporter genes in the progression of prostate cancer. Prostate 2016; 76: 434–444

[35] Antony F, Deantonio C, Cotella D et al. High-throughput assessment of the antibody profile in ovarian cancer ascitic fluids. Oncoimmunology 2019; 8: e1614856

[36] Zhang H, Wang Q, Gu J et al. Elevated mitochondrial SLC25A29 in cancer modulates metabolic status by increasing mitochondria-derived nitric oxide. Oncogene 2018; 37: 2545–2558

[37] Zhao Z, Zhan Y, Jing L et al. KLF10 upregulates ACSM3 via the PI3K/Akt signaling pathway to inhibit the malignant progression of melanoma. Oncol Lett 2022; 23: 175

[38] Sakaguchi S, Yamaguchi T, Nomura T et al. Regulatory T cells and immune tolerance. Cell 2008; 133: 775–787

[39] Ohue Y, Nishikawa H. Regulatory T (Treg) cells in cancer: can treg cells be a new therapeutic target? Cancer Sci 2019; 110: 2080–2089

[40] Liu ZZ, Han ZD, Liang YK et al. TRIB1 induces macrophages to M2 phenotype by inhibiting IKB-zeta in prostate cancer. Cell Signal 2019; 59: 152–162

[41] Li Y, Huang Q, Zhou Y et al. The clinicopathologic and prognostic significance of programmed cell death ligand 1 (PD-L1) expression in patients with prostate cancer: a systematic review and meta-analysis. Front Pharmacol 2018; 9: 1494

[42] Herbst RS, Baas P, Kim DW et al. Pembrolizumab versus docetaxel for previously treated, PD-L1-positive, advanced non-small-cell lung cancer (KEYNOTE-010): a randomised controlled trial. Lancet 2016; 387: 1540–1550

[43] Rowshanravan B, Halliday N, Sansom DM. CTLA-4: a moving target in immunotherapy. Blood 2018; 131: 58–67

[44] Waitz R, Solomon SB, Petre EN et al. Potent induction of tumor immunity by combining tumor cryoablation with anti-CTLA-4 therapy. Cancer Res 2012; 72: 430–439